Simulation of Droplet Jetting of a Non-Newtonian Mixed Suspension

Conference Paper · May 2016

CITATIONS
2

READS
150

5 authors, including:

Martin Svensson
Xylem Global Water Solution
2 PUBLICATIONS **9** CITATIONS
SEE PROFILE

Andreas Mark
Chalmers University of Technology
66 PUBLICATIONS **465** CITATIONS
SEE PROFILE

Fredrik Edelvik
Fraunhofer-Chalmers Centre
115 PUBLICATIONS **943** CITATIONS
SEE PROFILE

Andrzej Karawajczyk
Mycronic
10 PUBLICATIONS **138** CITATIONS
SEE PROFILE

Simulation of Droplet Jetting of a Non-Newtonian Mixed Suspension

Martin Svensson[1], Andreas Mark[1], Fredrik Edelvik[1], Andrzej Karawajczyk[2] and Gustaf Mårtensson[2*]

[1] *Fraunhofer-Chalmers Research Centre for Industustrial Mathematics*
Chalmers Science Park, SE-412 88 Göteborg, Sweden
martin.svensson@fcc.chalmers.se

[2] *Mycronic AB*
Nytorpsvägen 9, Box 3141, SE-183 03 Täby, Sweden
gustaf.martensson@mycronic.com

Abstract

The jet printing of a dense mixed non-Newtonian suspension is based on the rapid displacement of fluid through a nozzle, the forming of a droplet and eventually the break-off of the filament. The ability to model this process would facilitate the development of future jetting devices. The purpose of this study is to propose a novel simulation framework and to show that it captures the main effects such as droplet shape, volume and speed. In the framework, the time dependent flow and the fluid-structure interaction between the suspension, the moving piston and the deflection of the jetting head is simulated. The system is modelled as a two phase system with the surrounding air being one phase and the dense suspension the other. Hence, the non-Newtonian suspension is modelled as a mixed single phase with properties determined from material testing. The simulations were performed with two coupled in-house solvers developed at Fraunhofer-Chalmers Centre; IBOFlow, a multiphase flow solver and LaStFEM, a large strain FEM solver. Jetting behaviour was shown to be affected not only by piston motion and fluid rheology, but also by the energy loss in the jetting head. The simulation results were compared to experimental data obtained from an industrial jetting head.

Keywords: Multiphase flow, granular suspension, SMT, solder paste, jetting, computational fluid dynamics

1. Introduction

The development of electronic components are continuously pushing manufacturers to produce smaller and more densely packed components circuit boards. This rapid development could hardly been sustained without efficient, flexible and highly accurate manufacturing methods. Today's mounting methods are mainly based the surface-mount technology (SMT), possibly in combination with the through-hole technique. For SMT, the components are soldered onto the surface of the printed circuit board (PCB) compared to the through-hole technique where the wire leads are fitted into holes in the PCB. SMT was introduced in the 1960s, but is still developing, making it possible to decrease the size of the components, increase the density of components on the PCB and increase the production rate. Before the components can be mounted, solder paste is applied to the solder pads on the PCB. The components are then placed on their specific positions on the board and the PCB is heated so that the solder paste solidifies to form the solder joints.

The conventional method for applying the solder paste is to use a screen printing process. This technique is fast, but since a specific stencil is needed for every component pattern, the process is quite inflexible. An alternative method is to dispense the solder paste directly to the PCB with is more flexible and also less prone to rework, but is often considerably slower than screen printing. Mycronic is offering a non-contact jet printer where the solder paste is dispensed on the fly. In this way, the process becomes very flexible and at the same time fast, with dispensing rates at over one millions dots per hour. The driving force in the jet printer is a piezo element that expands rapidly when subjected to an electrical signal and causes the solder paste to accelerate through the nozzle of the printer head. The solder paste consists of a mixture of solid granules and flux which makes the rheology of the fluid different from Newtonian fluids. Due to structural reorganization of the granules when subjected to deformation, the solder paste exhibits shear thinning behaviour. This non-Newtonian behaviour is essential for the result of the jet printer. The solder jet printing technique requires knowledge of the flow conditions inside the printer head, how the material behaves under these conditions and which parameters that affect the droplet formation as the solder paste deposits from the printer head.

There are several studies to be found within the field of dispensing and droplet detachment. The different mechanisms that control the drop formation are described thoroughly by Clasen et al. [1]. Successful attempts have been made to simulate the drop formation of Newtonian fluids using a one dimensional formulation of the Navier-Stokes equations proposed by Eggers and Dupont [2]. This method was later used to accurately simulate the drop formation in the ink-jetting process [3, 4]. For non-Newtonian fluids, experimental studies of drop detachment in granular suspensions have been carried out by Bonnoit et al. [5]. Morrison and Harlen [6] uses the finite element method and an Eulerian-Lagrangian approach for simulating the droplet formation of viscoelastic fluids in the dripping flow regime, but when it comes to simulating solder paste in the jetting regime no previous work could be found.

In this study, a novel simulation framework is presented with the aim to capture the main characteristics of solder paste jetting and investigate how different parameters, associated with the printer head as well as the solder paste, affect the jetting behaviour. Specifically, the effect of the deformation of the printer head on the droplet velocity and the system's changes in the rheology model, are studied. The simulations are compared with experimental data from an industrial jetting head.

In Section 2, an overview of the computational model is given. A more detailed description of the numerical framework

[*] Support from the Swedish Research Council (contract 2010-4334) is gratefully acknowledged.

is presented in Section 3. The solder paste and the rheological model are described in Section 4. Results from the simulations are shown in Section 5 followed by some concluding remarks in Section 6.

2. Computational model

The computational domain consists of the lower part of the printing head. A schematic figure can be seen in Figure 1. The piston is treated as rigid, but the lower part of the chamber is allowed to deform. The piston is accelerated by a piezo electric element that expands rapidly when subjected to an electrical signal, and constrained by a system of springs. The motion of the piston is calculated prior to the flow simulations using a linear, orthotropic expansion model, that ensures a correct axial elongation and zero in plane expansion of the piezo. The rapid acceleration causes a pressure pulse in the chamber which forces the solder paste through the nozzle. At the same time, the pressurized fluid is interacting with the structure of the printer head causing it to deform. The deformation is assumed to be most prominent at the lower part of the chamber, depicted in Figure 1, thus this is the only deformable structure in the computational model. There is a back flow over the upper boundary during the jetting event. The actual magnitude of the this back flow is difficult to measure accurately during the jetting sequence, so in order to account for the flow, a porous pressure drop model is applied at the upper boundary of the fluid domain assuming that the pressure drop is caused by viscous forces. When the droplet leaves the nozzle the system is modelled as a two phase system with the surrounding air being one phase and the solder paste the other. Hence, the non-Newtonian suspension is modelled as a mixed single phase with properties determined from material testing. This study does not include the impact of the droplet on to the substrate, but is focusing on the droplet formation and separation.

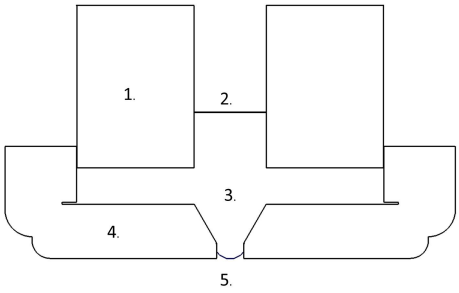

Figure 1: Schematic model of the jetting head. 1.) Moving piston (rigid body), 2.) Porous boundary, 3.) Chamber, 4.) Deformable part of the printer head, 5.) Meniscus position.

3. Numerical method

The motion of an incompressible fluid is governed by the Navier-Stokes equations,

$$\nabla \cdot \bar{u} = 0$$

$$\rho_f \frac{\partial \bar{u}}{\partial t} + \rho_f \bar{u} \cdot \nabla \bar{u} = -\nabla p + \mu \nabla^2 \bar{u},$$

where $\bar{u}$ is the fluid velocity, ρ_f is the fluid density, p is the pressure and μ is the apparent viscosity defined as the ratio between shear stress and shear rate, $\mu = \frac{\sigma}{\dot{\gamma}}$. The finite volume method is used to solve the Navier-Stokes equations. The equations are solved in a segregated way and the SIMPLEC method derived in [7] is used to couple the pressure and the velocity fields. All variables are stored in a co-located arrangement and the pressure weighted flux interpolation proposed in [8] is used to suppress pressure oscillations. Two-phase flows are modelled with the Volume of Fluid (VOF) method, where the local property of the fluid is dependent on the volume fraction. The volume fraction is transported with the local velocity field. To keep the interface between the solder paste and the air sharp, a hybrid CICSAM convective scheme is adopted [9]. The Continuum Surface Force derived in [10] is used to model the surface tension. A Cartesian octree grid is used for the spatial discretization of the fluid domain and dynamic refinements around moving objects and interfaces between phases in the flow are used.

Further, the immersed boundary method [11] is used to model the presence of moving solid objects, without the need of a body-fitted mesh. In the method, the fluid velocity is set to the local velocity of the object with an immersed boundary condition. To set this boundary condition, a cell type is assigned to each cell in the fluid domain. The cells are marked as fluid cells, extrapolation cells, internal cells or mirroring cells depending on the position relative to the immersed boundary. The velocity in the internal cells is set to the velocity of the immersed object with a Dirichlet boundary condition. The extrapolation and mirroring cells are used to construct implicit boundary conditions that are added to the operator for the momentum equations. This results in a fictitious fluid velocity field inside the immersed object. Mass conservation is ensured by excluding the fictitious velocity field in the discretized continuity equation. A thorough description of the method and an extensive validation can be found in [12].

The porous boundary condition is defined as a pressure jump described by Darcy's equation,

$$\Delta P = -\frac{\mu}{\alpha} v,$$

where μ is the viscosity and α is the permeability of the porous media.

The finite element method is used to solve the deformation of the jetting on an unstructured mesh. For spatial discretization, first order tetrahedral cells are used and for time discretization, the Newmark implicit second order method is employed. The fluid-structure interaction is handled iteratively using Gauss-Seidel iterations. The structural mesh of the lower part of the printer head can be seen in Figure 2 together with piston and the the pressurized chamber. Only a quarter of the printer head is included in the simulations due to axial symmetry.

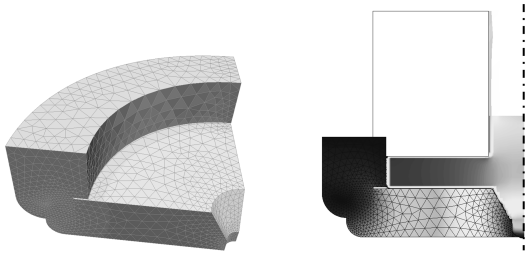

Figure 2: Geometrical model of the jetting head. In the left figure the deformable structure is shown separately and in the right figure it is shown together with the pressurized chamber and rigid piston.

4. Rheology

Solder paste is a non-Brownian suspension of metallic alloy granules and a carries fluid consisting of a complex mixture of

organic or inorganic resins. The granules are essentially spherical and have a Gaussian diameter distribution with a mean of approximately $20\,\mu m$. The suspension has a volume fraction by mass of 84%. The density of the suspension is $3.95\,kg/dm^3$ and the ratio of density between the granule alloy, ρ_m, and the carrier fluid, ρ_f, is $\rho_m/\rho_f = 8$.

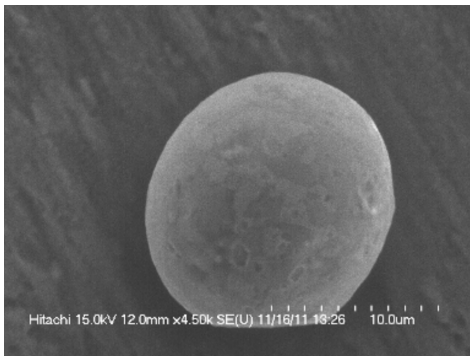

Figure 3: A SEM image of an individual granule of SuAgCu solder.

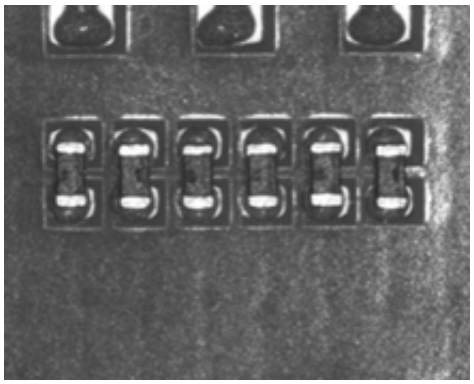

Figure 4: A photograph of six resistors mounted on individual solder paste deposits.

The solder paste is modelled as a Carreau fluid, see [13], where the apparent viscosity of the fluid is dependent on the local shear rate,

$$\mu = (\mu_0 - \mu_\infty)\left(1.0 + (\lambda\dot{\gamma})^2\right)^{0.5(N-1)} + \mu_\infty,$$

where γ is the shear rate and λ and N are material constants derived from experiments. The quantities μ_0 and μ_∞ are the zero-shear-rate viscosity and the infinite-shear-rate viscosity defined as

$$\lim_{\dot{\gamma}\to 0} \frac{\sigma_{xy}}{\dot{\gamma}_{xy}} = \mu_0$$

and

$$\lim_{\dot{\gamma}\to \infty} \frac{\sigma_{xy}}{\dot{\gamma}_{xy}} = \mu_\infty.$$

For very low or very high shear rates, the apparent viscosity of Carreau fluids approaches Newtonian plateaus, where the viscosity is independent of shear rate [14]. These plateaus are determined from the limit values μ_0 and μ_∞. In order to estimate the sensitivity of the system with respect to parameters in the rheology model, three different sets of parameters are tested. The parameters of the rheology model are shown in Table 1 and the model is shown in Figure 5, together with experimental data from a Couette rheometer and a Capillary rheometer. It should be mentioned that only the shear viscosity is included in the simulations.

Table 1: Carreau model parameters.

Parameter	Unit	Set 1	Set 2	Set 3
μ_0	Pa s	2.75e4	2.75e4	5.04e8
μ_∞	Pa s	52.28	18.00	4.00
λ	s	54.00	54.00	−1.43e8
N	-	−0.002	0.050	0.276

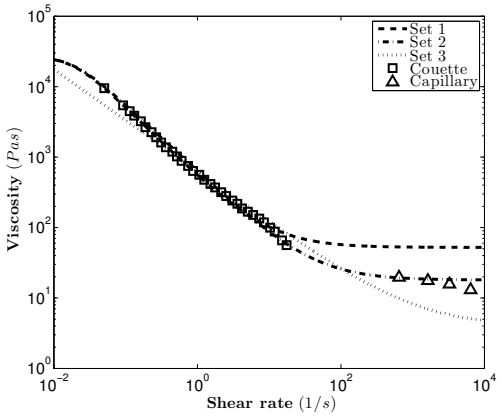

Figure 5: Viscosity for three different Carreau parameters compared to experimental data from a Couette- and a Capillary rheometer.

5. Results

The simulations are compared with images from an experimental set up where two subsequent images are taken with a $5\,\mu s$ interval. In this way, the position and the velocity is obtained. This is done for five different times, 30, 35, 40, 45 and $50\,\mu s$, so that the evolution of the droplet can be observed. The positions and velocities are averaged over a large set of droplets in excess of 300 images. The results from the simulations are presented in a similar manner, but the times for the snapshots are shifted $10\,\mu s$ to 20-40 instead, in order to obtain corresponding results. The reason for this is probably an effect of a time delay in the experimental set up and is considered not to influence the credibility of the simulations notably. In the simulations, rheology Set 1 is used. The results from the simulations are shown together with images from the experimental data in Figure 6. It can be seen that the droplet shape from the simulations correspond well with the experiments. However, the filament thinning is more prominent in the simulations (this is most clear in the last snapshot). The thickness of the droplet follows the motion of the piston very closely in the simulations and at the time of the last snapshot the piston is rapidly retracting which cause the filament to stretch. This can also be seen in experiments but here it is more continuously thinning. The reason for the difference might be due to the

fact the solder paste is modelled as a continuous phase and that the solder paste is behaving differently under extensional flow or that the rheology model only account for shear viscosity. If the viscosity would have been higher under extensional flow, the filament thinning would have been slower and possibly closer to the experiments.

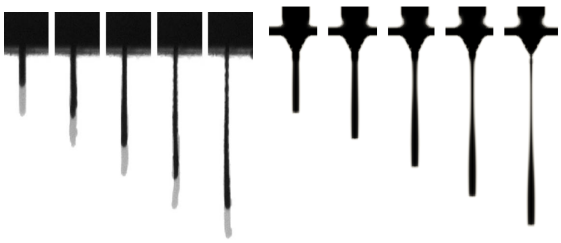

Figure 6: Snapshots of the droplet evolution from experimental data (left) and from simulations (right) at five different time steps.

In order to study effect of how the deformation of the printer head influences the simulated droplet velocity, a completely rigid printer head is compared with a printer head where the lower plate is allowed to deform as described in Section 3. The droplet velocity of the two different cases is shown in 7 and the pressure in the middle of the chamber is shown in Figure 8. The velocity of the droplet is approximately 20% higher for the stiff geometry then for the deformable one. When studying the pressure in the chamber for the stiff printer head it can be seen that it is fluctuating with a larger amplitude since the deformation is not present to dampen the pressure peaks. The increased pressure is affecting the acceleration phase and is causing the droplet to travel faster for the simulation with a stiff geometry then with a deformable one.

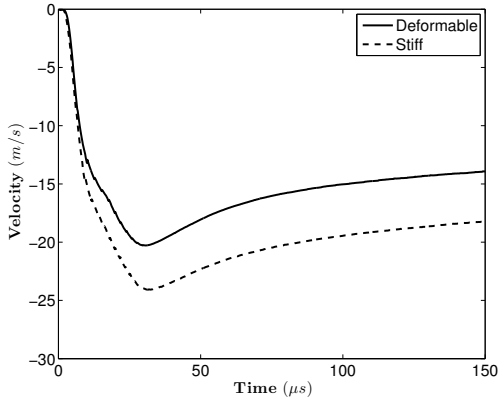

Figure 7: Droplet velocity for the deformable printer head compared to the stiff printer head.

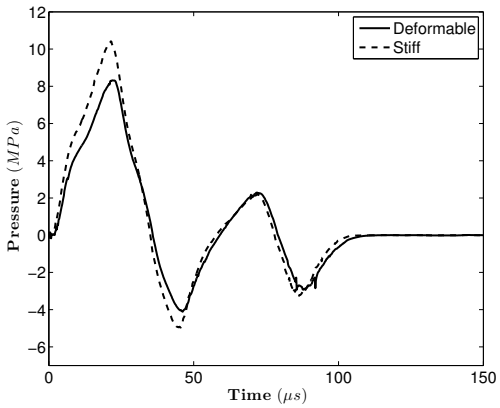

Figure 8: Pressure in the middle of the chamber for the deformable printer head compared to the stiff printer head.

The rheology of the solder paste is of great importance for the success of the jetting. To obtain an estimate of the sensitivity of the rheology model, the jetting behaviour of three different parameter sets, described in Section 4, are compared and the result is shown in Figure 9. Two observations can be made from this comparison. Firstly, the velocity of the droplet differs between droplets A, B and C. For droplet A, which has the highest velocity, the infinite-shear-rate viscosity is higher than the other two. Intuitively, the high viscosity would lead to a low velocity but since the pressure drop model at the upper boundary is proportional to the viscosity, instead the pressure in the chamber is increased, leading to a higher droplet velocity. Secondly, the shape of the droplets are different due to the difference in the rheology model. Droplet A is long an slender, droplet B is thicker and droplet C is significantly thicker and more drop shaped. This effect may be explained by the viscosity difference in the shear region where the forming of the droplet takes place. For the droplet with higher viscosity, the fluid leaving the nozzle is pushing the droplet head forward rather then to coalesce and form a more compact droplet. Another explanation for the difference in droplet shape, is that the higher chamber pressure for droplet A, due to a lower infinite-shear-rate viscosity, results in an initially stronger acceleration of solder paste. This leads to a velocity distribution within the droplet that is more homogeneous then for the droplet with a higher infinite-shear-rate velocity, meaning that the body of the droplet will not catch up with the head as easily.

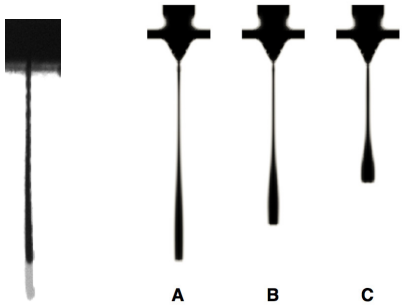

Figure 9: Droplet shapes for three different Carreau model parameters (right) compared to the experimental droplet shape (left). The leftmost simulated droplet, A, employ parameter set 1, the droplet in the centre, B, parameter set 2 and the rightmost droplet, C, parameter set 3.

6. Conclusions

It is shown in this project that the proposed framework can be used to simulated and capture different properties of the jetting sequence. A qualitative comparison is presented with the knowledge that the porous boundary condition is an approximation. However, the droplet velocity can be fitted to experimental data and the shape of the simulated droplet corresponds well with experiments.

When comparing the simulation where the printer head is allowed to deform to the simulation with a stiff printer head, it is concluded that the deformation affects the pressure, and therefore also the droplet velocity, negatively and that the effect is significant, approximately 25% for the pressure and 20% for the droplet velocity.

It is clear that different parameters in the rheology model affect the properties of the droplet. The low shear rate region affects the form of the droplet head, while the droplet velocity is mainly affected by the high shear rate region. Surprisingly, the velocity is highest for parameter set 1 with the highest infinite-shear-rate viscosity. This can be explained by the properties of the upper boundary condition since the pressure drop over the porous media is related to the viscosity of the fluid. A high viscosity therefore generates an increased pressure in the chamber which is sufficiently large to overcome the higher internal resistance of the material itself.

For further studies of the jetting behaviour and droplet formation of a non-Newtonian mixed suspension, the identification of other important parameters, such as geometrical properties of the jetting head and meniscus position of the solder paste, is suggested. It is also advised to validate the simulations against different types of experimental measurements, such as pressure in the chamber or deflection of jetting head. Mycronic is currently using the framework to understand the mechanisms of jetting and find the most important parameters for the jetting behaviour.

References

[1] Clasen, C., Phillips, P.M., Palangetic, L. and Vermant, J., Dispensing of rheologically complex fluids: The map of misery. *AIChE Journal*, 58(10):3242–3255, 2012.

[2] Eggers, J. and Dupont, T.F., Drop formation in a one-dimensional approximation of the navier–stokes equation. *Journal of fluid mechanics*, 262:205–221, 1994.

[3] Driessen, T. and Jeurissen, R., A regularised one-dimensional drop formation and coalescence model using a total variation diminishing (tvd) scheme on a single eulerian grid. *International Journal of Computational Fluid Dynamics*, 25(6):333–343, 2011.

[4] van der Bos, A., van der Meulen, M-J., Driessen, T., van den Berg, M., Reinten, H., Wijshoff, H., Versluis, M. and Lohse, D., Velocity profile inside piezoacoustic inkjet droplets in flight: comparison between experiment and numerical simulation. *Physical review applied*, 1(1):014004, 2014.

[5] Bonnoit, C., Bertrand, T., Clément, E., and Lindner, A., Accelerated drop detachment in granular suspensions. *Physics of Fluids*, 24(4):043304, 2012.

[6] Morrison, N.F. and Harlen, O.G., Viscoelasticity in inkjet printing. *Rheologica Acta*, 49(6):619–632, 2010.

[7] Van Doormal J. and Raithby, G.D., Enhancement of the simple method for predicting incompressible flows. *Numerical Heat Transfer*, 7:147–163, 1984.

[8] Rhie, C.M. and Chow, W.L., Numerical study of the turbulent flow past an airfoil with trailing edge separation. *AIAA J1*, 21:1527–1532, 1983.

[9] Ubbink, O., Numerical prediction of two fluid systems with sharp interfaces, 1997. PhD. Thesis, Department of Mechanical Engineering, Imperial College of Science, London, United Kingdom.

[10] Brackbill, J.U., Kothe, D.B. and Zemach, C., A continuum method for modeling surface tension. *J. Comp. Phys.*, 100:335–354, 1992.

[11] Mark, A. and van Wachem, B.G.M., Derivation and valdiation of a novel implicit second-order accurate immersed boundary method. *J. Comput. Phys.*, 227:6660–6680, 2008.

[12] Mark, A., Rundqvist, R. and Edelvik, F., Comparison between different immersed boundary conditions for simulation of complex fluid flows. *Fluid Dynamics & Materials Processing*, 7(3), 2011.

[13] Bird, R.B., Armstrong, R.C., and Hassager, O., *Dynamics of polymer liquids*. vol. 1, 2nd ed. Wiley, New York, 1987.

[14] Chhabra, R.P., *Rheology of Complex Fluids*, chapter Non-Newtonian Fluids: An Introduction, pages 3–34. Springer, New York, 2010.